

Effect of Heat Treatment on the Lithium Ion Conduction of the LiBH₄–LiI Solid Solution

Dadi Sveinbjörnsson,[†] Jon Steinar Gardarsson Myrdal,^{†,‡} Didier Blanchard,[†] Janet Jonna Bentzen,[†] Takumi Hirata,[§] Mogens Bjerg Mogensen,[†] Poul Norby,[†] Shin-Ichi Orimo,[§] and Tejs Vegge*,[†]

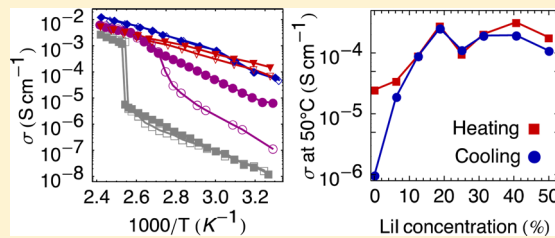
[†]Department of Energy Conversion and Storage, Technical University of Denmark, Frederiksbergvej 399, P.O. Box 49, DK-4000 Roskilde, Denmark

[‡]Center for Atomic-Scale Materials Design, Department of Physics, Technical University of Denmark, Anker Engelunds Vej 1, DK-2800 Lyngby, Denmark

[§]Institute for Materials Research, Tohoku University, 2-1-1 Katahira, Aoba-ku, Sendai 980-8577, Japan

Supporting Information

ABSTRACT: The LiBH₄–LiI solid solution is a good Li⁺ conductor and a promising crystalline electrolyte for all-solid-state lithium based batteries. The focus of the present work is on the effect of heat treatment on the Li⁺ conduction. Solid solutions with a LiI content of 6.25–50% were synthesized by high-energy ball milling and annealed at 140 °C. Powder X-ray diffraction and scanning electron microscopy were used for characterizing the samples and for comparing their crystallite sizes and the density of defects before and after the annealing. The Li⁺ conductivity was measured using impedance spectroscopy, resulting in conductivities exceeding 0.1 mS/cm at 30 °C and 10 mS/cm at 140 °C. It was found that the formation of defect-rich microstructures during ball milling increased the specific conductivities of these compounds significantly. The phase transition temperatures between the orthorhombic and hexagonal structures of LiBH₄ were measured using differential scanning calorimetry (DSC). The measured transition temperatures range from 100 to –70 °C and show a linear decrease of 70 °C for every 10% of LiI addition up to a LiI content of 25%. The relative stability of the two structures was calculated using density functional theory, and together with the DSC measurements, the calculations were used to evaluate the change in entropic difference between the structures with LiI content.



1. INTRODUCTION

Lithium battery research is growing ever more important as the need for more efficient and more sustainable methods for energy storage continues to grow rapidly. This is in particular true for the energy and transportation sectors. Today, the primary application of lithium batteries is in the portable electronics sector. But, when it comes to applications in systems on a larger scale, existing battery technologies fall short on price, energy density, safety, and charge–discharge cycle lifetime. Commercial Li ion batteries use flammable organic liquid or gel electrolytes. Their main attractive property is their high Li⁺ conductivity. Examples of such electrolytes include 1 M LiPF₆ in EC-DMC (organic liquid, 12 mS/cm at 27 °C),¹ 1 M LiBF₄–EMIBF₄ (ionic liquid, 9 mS/cm at 27 °C)² and 1 M LiPF₆ in EC-DMC and PVDF-HFP (gel, 3 mS/cm at 27 °C).¹ However, the main disadvantage of such electrolytes is their inflammability, which causes safety issues that only grow worse as the demands on the energy density of the systems increase.^{3,4} Furthermore, the usage of liquid or gel electrolytes can result in diminished cell capacity and limited charge–discharge cycle life due to dendrite formation at the electrode–electrolyte interface.⁵

Replacing the currently used liquid and gel electrolytes with solid-state electrolytes would enhance the safety and extend the cycle life of the batteries. However, designing a suitable solid electrolyte material with sufficient chemical and electrochemical stability, as well as offering a sufficiently high lithium ion conduction and negligible electronic conduction, remains a challenge.⁶

Various types of crystalline solid-state Li⁺ conducting materials are known.³ Among these are Li₃N,⁷ perovskite type oxides such as lithium lanthanum titanate (LLTO),^{8–11} garnet-type structures such as Li₆BaLa₂Ta₂O₁₂,¹² NASICON-type structures,^{13,14} LISICON-type structures,¹⁵ and Li₁₀GeP₂S₁₂.¹⁶ However, there are some problems with the usage of many of these materials as solid electrolytes in lithium batteries. The decomposition voltage of Li₃N is too low for practical use. LLTO and NASICON are not stable in contact with elemental lithium, and reducible Ti₄⁺ ions make the electronic conductivity of LLTO too high.¹⁷ The Li⁺

Received: October 10, 2012

Revised: January 18, 2013

Published: January 30, 2013

conductivity of LISICON is rather low and in some cases decreases with time.¹⁸

A Li⁺ conductivity of at least 1 mS/cm is often mentioned as the minimum conductivity required for an electrolyte to work well in consumer batteries.^{19,20} The conductivity of the above-mentioned crystalline solid electrolytes is considerably lower than this, with the exception of Li₁₀GeP₂S₁₂ that has a Li⁺ conductivity of 12 mS/cm at 27 °C.¹⁶ The search for other crystalline electrolyte materials with Li⁺ conductivities above 1 mS/cm is of both fundamental and practical interest for secondary lithium battery research.

Lithium borohydride, LiBH₄, is lightweight (0.666 g/cm³) and has been investigated extensively as a possible hydrogen storage material.^{21–27} In recent years, lithium borohydride has also gained increased attention as a potential crystalline solid electrolyte material for lithium batteries.^{28–30} At room temperature, LiBH₄ has a poorly Li⁺ conducting orthorhombic crystal structure (*Pnma*, approximately 10⁻⁸ S/cm at 30 °C), but around 110 °C, it undergoes a reversible structural transition to a highly Li⁺ conducting hexagonal structure (*P6₃mc*, approximately 1 mS/cm at 120 °C).^{28,31} In the following, the two polymorphs will be referred to as the LT phase (orthorhombic) and HT phase (hexagonal), respectively. LiBH₄ is an electrical insulator in both structures, with calculations showing a large band gap of approximately 6.7 eV.^{32,33} A working all-solid-state battery cell using LiBH₄ in the HT phase as an electrolyte has recently been reported.³⁴

The HT phase of LiBH₄ can be stabilized at room temperature by adding lithium halides (LiI, LiBr, and LiCl), with the LiI addition giving the best Li⁺ conduction results.³⁵ It should be noted that the low-temperature modification of LiI below 0 °C, known as β-LiI, has a *P6₃mc* structure³⁶ and is thus isostructural with the HT phase of LiBH₄. The LiBH₄–LiI system forms a solid solution,³⁷ and studies on its structure and properties have recently been published. Rude et al.³⁸ have investigated the LiBH₄–LiI solid solution as a hydrogen storage material, and Miyazaki et al.³⁹ have studied its properties as a Li⁺ conductor.

In the present work, we present a systematic study on the (1 – *x*)LiBH₄+*x*LiI solid solutions: on their crystalline structure, Li⁺ conduction properties, relative phase stabilities, and phase transition temperatures for a wide range of LiI content *x*. In a continuation and complementary to the work of Miyazaki et al.,³⁹ the present work provides a thorough understanding of the correlations between LiI content, microstructure, and Li⁺ conductivity, as well as addressing phase stabilities and entropic behavior. The aim is both to provide a fundamental understanding of the microstructural properties of the solid solution and to address the more practical question of how its Li⁺ conductivity can be optimized. The results are based both on experimental work and on density functional theory calculations.

2. EXPERIMENTAL SECTION

2.1. Synthesis. LiBH₄ powder (purity 95%) and LiI beads (purity 99%) were purchased from Alfa Aesar Co. The (1 – *x*)LiBH₄+*x*LiI samples were synthesized by planetary ball milling under Ar atmosphere. Pure LiBH₄ was also ball milled for comparison. In each milling, a stainless steel vial with an inner volume of 250 mL was rotated at 650 rpm for 2 h using a Fritsch Pulverisette P6. A total of 2 g of precursor powder was inserted into the vial for each milling. Twenty-five tungsten carbide balls were used, and the sample to ball mass ratio was

1/100. No contamination from the milling vial or the balls was found in the diffraction patterns of the milled samples.

For the sample used in the impedance spectroscopy temperature cycling measurement (see Figure 7), the procedure was the same as described above, except that a total of 0.5 g of precursor powder was rotated in a 45 mL vial on a Fritsch Pulverisette P7. Here, the sample to ball mass ratio was 1/180.

2.2. Powder X-ray Diffraction. After ball milling, the samples were characterized using a Cu K α Bruker D8 diffractometer with a Bragg–Brentano geometry and a LynxEye detector, operating at 40 kV and 40 mA. All X-ray diffraction (XRD) measurements were performed at room temperature and under Ar atmosphere using an airtight polyethylene sample holder from Bruker Co. The exposure time was 3 s/step with a step size of 0.02°. The measurements were performed using a variable slit size. After the measurement, the data intensity was corrected for the variable slit size and the K $\alpha 2$ signal was subtracted.

A fraction of each sample was annealed in a furnace at 140 °C for 70 h. XRD measurements were subsequently performed on the annealed powder in order to detect, by comparison with the nonannealed powder, the anticipated sintering effect of the heat treatment.

The diffraction peak positions were found using the GSAS refinement software. The full width at half-maximum (fwhm) of the diffraction peaks was calculated using the peak fitting software FITYK.⁴⁰ The contributions to the fwhm from the crystallite size and from the crystallographic defects were separated by fitting the size and strain parameters in

$$B(\theta) = \sqrt{\left(\frac{k\lambda}{D \cos \theta}\right)^2 + (4\eta \tan \theta)^2 + B_0^2} \quad (1)$$

to the measured fwhm values in each diffractogram. This expression for the peak broadening is a combination of the Scherrer equation for size broadening⁴¹ and the Stokes and Wilson expression for strain broadening,⁴² where *D* is the average crystallite size and η is the strain. The shape factor *k* was assumed to be 0.9, and the instrumental broadening *B*₀ was 0.01.

2.3. Scanning Electron Microscopy. The microstructure was characterized using a JEOL 840 scanning electron microscope (SEM) with an acceleration voltage of 10 kV. The samples were transferred under vacuum from the glovebox to the microscope using a portable vacuum transference system.

2.4. Impedance Spectroscopy. The conductivity of the samples was determined by AC impedance spectroscopy using a PARSTAT 2273 potentiostat. The ball-milled powder was pressed into pellets with a diameter of 13 mm and a thickness of approximately 2.5 mm. Lithium foil was placed onto both faces of the pellets as electrodes. The powder and the lithium foil were pressed simultaneously at 1 ton/cm². The porosity of the pellets was estimated to be around 0.5. All preparation and measurements were carried out under Ar atmosphere. The frequency range of the impedance measurements was set from 100 mHz to 1 MHz. The samples were heated up from 30 to 140 °C in steps of 5 or 10 °C and then cooled back down to 30 °C using the same step size. The samples were equilibrated at a constant temperature for at least 40 min prior to each measurement.

For the measurement of the conductivity of the $\frac{1}{2}$ LiBH₄+ $\frac{1}{2}$ LiI sample during five heating and cooling cycles (see Figure 7), a Hioki 3532-80 potentiostat was used, and the

pellet dimensions were 8 mm in diameter and 0.9 mm in thickness.

2.5. Differential Scanning Calorimetry. The phase transition temperatures of the $(1 - x)\text{LiBH}_4 + x\text{LiI}$ samples were determined by differential scanning calorimetry (DSC), using a Netzsch DSC 200 F3 calorimeter. For each measurement, 10 mg of sample was sealed in an aluminum crucible under Ar atmosphere. The samples were heated from room temperature to 140 °C at 2 °C/min, kept at 140 °C for 30 min, and thereafter, cooled to −170 °C at 2 °C/min. A liquid nitrogen cryostat was used to control the temperature.

3. COMPUTATIONAL SECTION

Calculations were performed using density functional theory as it is implemented in the Vienna Ab-initio Simulation Package (VASP)⁴³ with a plane wave basis set. For exchange and correlation, we used the PBE functional.⁴⁴ All lithium electrons were included in the calculation, but for nonvalence boron electrons, we used the projector augmented wave method (PAW).^{45,46} The energy cutoff was set to 350 eV, and a $4 \times 4 \times 4$ Monkhorst–Pack k-point mesh was used. The preparation of atomic structures and the setup of computational parameters was performed using the atomic simulation environment (ASE).⁴⁷

The ground-state energy for the $(1 - x)\text{LiBH}_4 + x\text{LiI}$ system was calculated for seven different values of x , that is, $x = 0, \frac{1}{16}, \frac{1}{8}, \frac{3}{16}, \frac{1}{4}, \frac{1}{2}$, or 1, both in the LT ($Pnma$) and HT ($P6_3mc$) crystal structures of LiBH_4 . For structural optimization, all atomic forces were relaxed down below 0.01 eV/Å.

4. RESULTS AND DISCUSSION

4.1. Density Functional Theory. Figure 1 shows the calculated energy difference between the $P6_3mc$ (HT) and

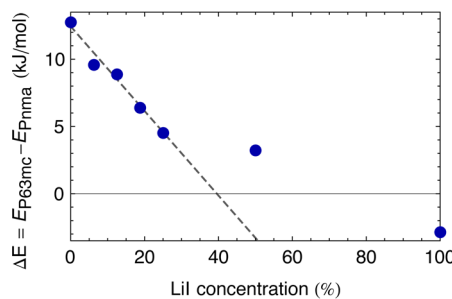


Figure 1. Ground-state energy difference between the $P6_3mc$ (HT) and $Pnma$ (LT) structures of LiBH_4 as a function of the content of LiI that has been substituted into the system. The stabilization of the HT structure relative to the LT structure is approximately linear up to a LiI content of 25%. The dotted line shows a linear fit of the data points for LiI contents from 0% to 25% to emphasize this.

$Pnma$ (LT) structures as a function of LiI content in the $(1 - x)\text{LiBH}_4 + x\text{LiI}$ system. Up to a LiI content of 25%, there is a close to linear stabilization with increasing LiI content, about 33 kJ/mol of I. There seems to be little addition in stability by going from 25% LiI content to 50%, but for pure LiI, the HT structure has become more stable than the LT structure. However, this increased stability of the HT structure versus the LT structure is a poor indicator of the real HT stability for pure LiI because the LT structure of LiBH_4 is not the ground-state structure of LiI. Nonetheless, we do believe that, for smaller iodine contents, the ground-state energy calculations give a

good estimate of the real stabilization in the $(1 - x)\text{LiBH}_4 + x\text{LiI}$ system, since we expect them to have a similar entropy behavior as a function of temperature. This claim is supported further in Section 4.5 by comparing the calculation results with the results of DSC measurements.

4.2. X-ray Diffraction. The diffraction patterns of both the annealed and the nonannealed $(1 - x)\text{LiBH}_4 + x\text{LiI}$ samples are shown in Figure 2. A diffraction pattern of nonannealed LiBH_4 that has been ball milled for 2 h is also shown for comparison. The pure ball-milled LiBH_4 has the LT structure, while the sample with 6.25% LiI is a blend of the LT and HT structures. For all samples with LiI content equal to or greater than 12.5%, only the HT phase is detected.

The positions of the reflections from the crystallographic planes ($hk0$), parallel to the hexagonal plane, are only slightly shifted to higher values when the LiI content is increased, reflecting a small expansion of the a axis with increased LiI content. The c axis, perpendicular to the hexagonal plan, is found to shrink with increasing LiI content up to 30% and then to expand with increasing LiI content between 30% and 50% (see Figure 2, in which a line is drawn to emphasize the shift of the (002) reflection).

The evolution of the lattice parameter c is plotted as a function of the LiI content in Figure 3a. The nonmonotonic evolution of the c axis is unexpected, and the contraction of c with increasing LiI content below a LiI content of 30% differs from what has previously been reported by Miyazaki et al.³⁹ For a LiI content above 30%, the c axis expands as expected when compared with the unit cell parameters of the hexagonal phases of pure LiBH_4 and pure LiI, respectively, and is in agreement with the values reported by Miyazaki et al.³⁹ and Rude et al.³⁸

One possible explanation for this behavior is the presence of solid solutions containing different amounts of iodine and different lattice constants that merge into one upon heating as reported by Rude et al.³⁸ Another possibility is the existence of some intermediate phases as described by Oguchi et al.³⁷ These effects could be the origin of the very asymmetric peak shapes and large peak broadening visible in Figure 2 for low LiI content. Such broadening at low LiI content is also visible in the diffraction patterns of refs 25 and 26.

Sintering and/or annealing effects are observed for the annealed LiBH_4 –LiI solid solutions in the form of narrower peaks for the annealed samples than for the nonannealed ones. However, the peculiar behavior of the c axis is still present in the annealed samples. As an example of the peak sharpening, the evolution of the fwhm of the (002) reflection with LiI content is shown in Figure 3b. The fwhm of the nonannealed powder varies with the LiI content and has a minimum at around 30% LiI content. This is also the LiI content for which the cell parameter c (see Figure 3a) is closest to the value reported for the cell parameters of pure LiBH_4 .³¹ After the annealing, the fwhm values are almost independent of the LiI content.

The broadening contribution from the strain and the crystallite sizes was analyzed using eq 1. This analysis was performed on the fwhm of four to six peaks depending on the diffraction patterns. Due to the limited quality of the data, no absolute values for D and η are reported herein. However, their relative contribution and evolution will be commented on in connection with the LiI content and the effect of the annealing.

It was found that, before the annealing, the broadening due to the strain is dominant over the size effect up to a LiI content of 25%. Knowing that the fwhm values are larger for the sample

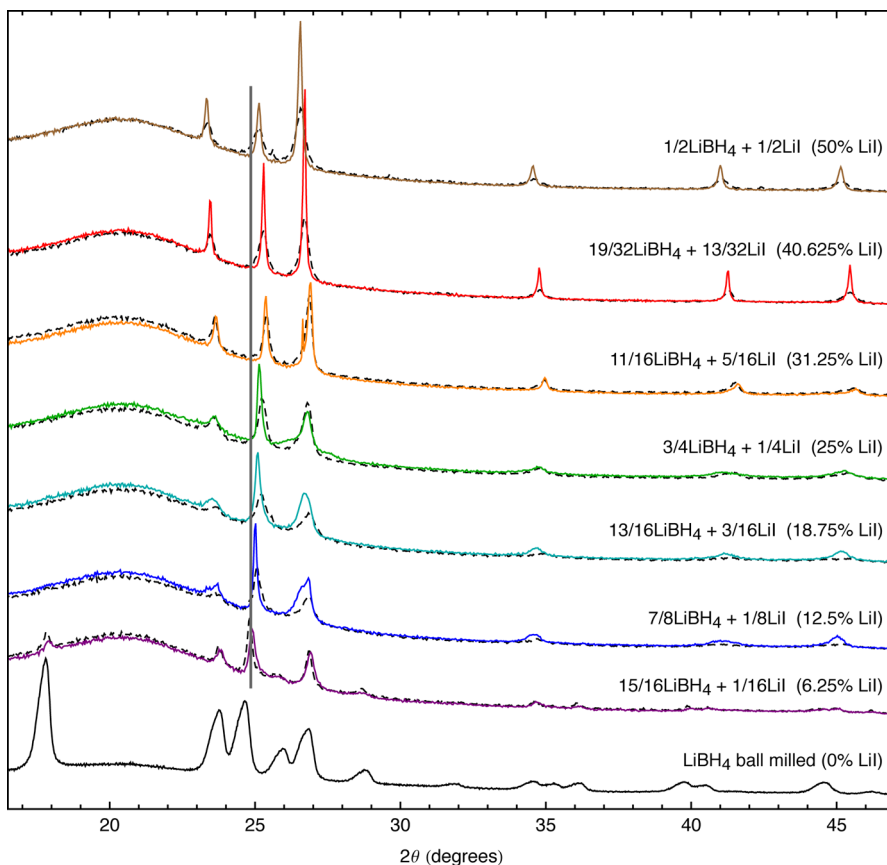


Figure 2. XRD patterns of $(1 - x)\text{LiBH}_4 + x\text{LiI}$ solid solutions. The black, dashed lines show diffraction patterns of nonannealed samples, and the colored, solid lines show diffraction patterns of samples that have been annealed at $140\text{ }^\circ\text{C}$ for 70 h. The black, solid line shows the diffraction pattern of pure ball-milled, nonannealed LiBH_4 for comparison. The vertical line at around 25° is drawn to emphasize the shift of the (002) reflection with LiI content. All measurements were performed at room temperature. The broad bump at the lowest angles is due to the polyethylene sample holder. The intensity of the diffraction pattern of pure LiBH_4 has been scaled down by $1/3$ in order to better fit the intensities of the remaining patterns in the figure. The molar percentage of LiI is shown in parentheses after the sample name for easier comparison with other figures in this work.

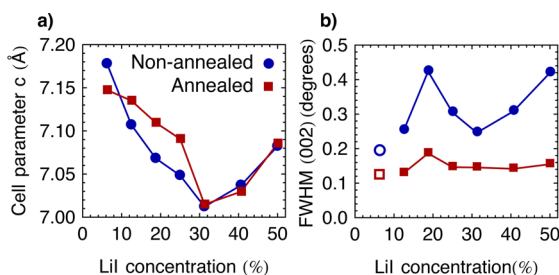


Figure 3. (a) Evolution of the unit cell parameter c in $(1 - x)\text{LiBH}_4 + x\text{LiI}$ with LiI content. (b) The fwhm of the (002) reflection of the $(1 - x)\text{LiBH}_4 + x\text{LiI}$ diffraction patterns as a function of LiI content. The fwhm of the samples with 6.25% LiI content are shown with empty dots; their values are not reliable because of overlapping diffraction peaks from the LT and HT structures of LiBH_4 .

with 18.75% LiI content than for samples with a higher content of LiI , the density of defects is greater for the former than for the latter. After annealing, the strain values are smaller and almost independent of the LiI content. Furthermore, the crystallite sizes of the annealed powders are found to be around three times greater than those of the nonannealed powders for samples with LiI contents larger than 25%. Overall, the fwhm are found to be lowered by the heat treatment.

It should be noted that the difference in strain before and after the annealing is found to be smallest for the sample with 30% LiI content, which is the LiI content at which the minima in the cell parameter c and the fwhm before annealing are observed (see Figure 3). It should also be noted that the sample with 6.25% LiI content contains two coexisting structures with overlapping diffraction peaks at the position of the (002) reflection of the HT phase. Therefore, the measured fwhm values are probably not accurate for this sample and have been left out for this analysis.

4.3. Scanning Electron Microscopy. Figure 4 shows SEM images of $1/2\text{LiBH}_4 + 1/2\text{LiI}$ powder. The sample in Figure 4a was ball milled (as described in Section 2.1) but did not receive any heat treatment. The sample in Figure 4b was ball milled and annealed in a furnace at $140\text{ }^\circ\text{C}$ for 70 h. A comparison of the two images shows that sintering does occur during the heat treatment, as the average size of the particles and the agglomerates in the powder are larger after the annealing than before it. This supports the results on the fwhm of the XRD data shown in Figures 2 and 3b.

4.4. Conductivity. The impedance spectroscopy measurements resulted in a Nyquist plot showing a single arc. The explanation for this can either be that only one contribution to the conduction is present or that two or more arcs, each corresponding to concurrent bulk and/or grain boundary

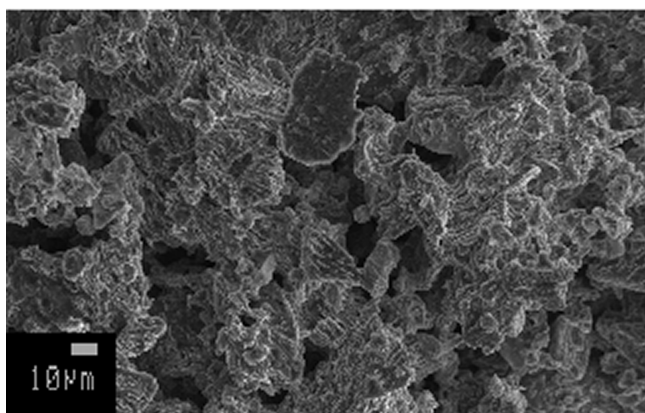
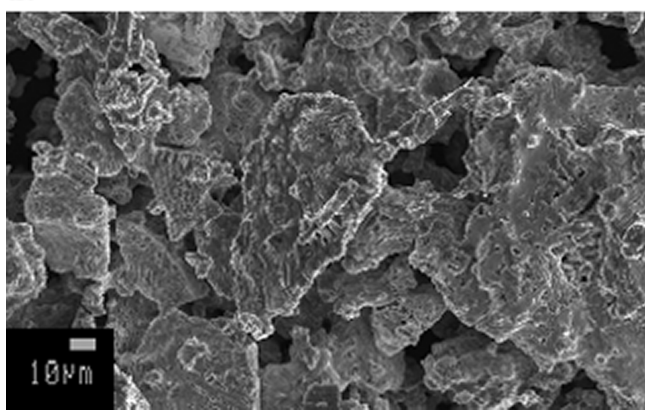
a)**b)**

Figure 4. SEM images of $\frac{1}{2}\text{LiBH}_4 + \frac{1}{2}\text{LiI}$. The scale in the lower left corner of the images shows the length of 10 μm . (a) After ball milling but before annealing. (b) After ball milling and annealing. It is clear that the average particle and agglomerate sizes are larger in the annealed sample than in the nonannealed sample.

contributions, overlap completely in the Nyquist plots. In such a case, however, it is not possible to separate the contributions from the bulk and the grain boundary conductivities using only impedance spectroscopy.^{48,49} Therefore, the conductivity values presented in the following are to be taken as the total conductivity of the sample. No contribution to the Nyquist plots from the Li electrodes was observed. The Nyquist plots were all fitted using an (RQ) equivalent circuit model, that is, a resistor and a constant phase element in parallel. The conductivity of the samples is given by

$$\sigma = \frac{d}{AR} \quad (2)$$

where R is the resistance obtained from the fit, d is the thickness of the sample, and A is its area.

Figure 5 shows an Arrhenius plot of the Li^+ conductivities measured for the different samples during heating and cooling (Nyquist plots and additional Arrhenius plots can be found in the Supporting Information). The pellets consisted of the as-milled powders, and the measurements were performed while first heating the pellets from room temperature to 140 °C and then cooling them back down to room temperature. The $(1 - x)\text{LiBH}_4 + x\text{LiI}$ solid solutions show very high ionic conductivity, with the sample with 40% LiI content exceeding 0.1 mS/cm at

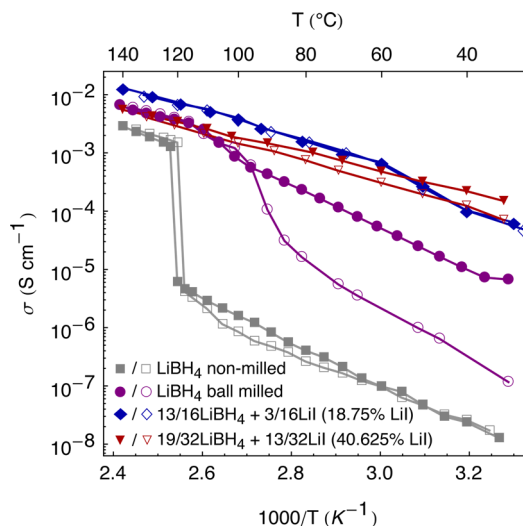


Figure 5. Li^+ conductivities of pure LiBH_4 , both ball-milled and nonmilled, and of two mixing ratios of $(1 - x)\text{LiBH}_4 + x\text{LiI}$, obtained from impedance spectroscopy. For each sample, the filled symbols denote heating runs, and the empty symbols denote cooling runs.

30 °C and the 18.75% LiI containing sample exceeding 10 mS/cm at 140 °C.

Generally, the slopes of the Arrhenius plots vary with both LiI content and temperature. There is a general trend that the slope of the plots decreases with increasing LiI content. This indicates that the activation energy of the Li^+ conduction decreases with increasing LiI content. Furthermore, as a result of the decreasing slopes with increasing LiI content, the samples with a low LiI content generally have a higher Li^+ conductivity at the highest measured temperatures than the samples with high LiI content.

Ball milling and heat treatment of the samples are also important for their conductivity. The as-received (nonmilled) LiBH_4 is in its poorly conducting LT phase. At around 120 °C, the sample changes to the HT phase, and the conductivity increases by more than 2 orders of magnitude, as expected.²⁸ This trend in the conductivity is fully reversible upon cooling, with a very small hysteresis. The ball-milled LiBH_4 is also in the poorly conducting LT phase (see Figure 2). However, defects arising during the ball milling may open up new Li^+ conduction pathways. This causes an increase in conductivity by almost 3 orders of magnitude close to room temperature, compared to the nonmilled LiBH_4 . When the ball-milled LiBH_4 is heated up above the phase transition temperature, it takes on the HT structure, presumably mending some of the defects caused by the ball milling. The return to the LT phase when cooling the sample down should mend the defects even further. Some of the conduction pathways present during the heating run are then closed as illustrated by the large fall of the conductivity between the heating and the cooling runs. After the thermal treatment, however, the sample is not defect-free, and the conductivity of the ball-milled sample is still higher than that of the as-received LiBH_4 .

The conductivity values at 50 °C are shown as a function of the LiI content in Figure 6. This temperature is chosen because it represents an approximate temperature at which a lithium battery could be operated. At 50 °C, the conductivity is 0.3 mS/cm for LiI contents of 18% and 40%. Although this temperature is at the upper limit of consumer battery usage, the LiBH_4 -LiI

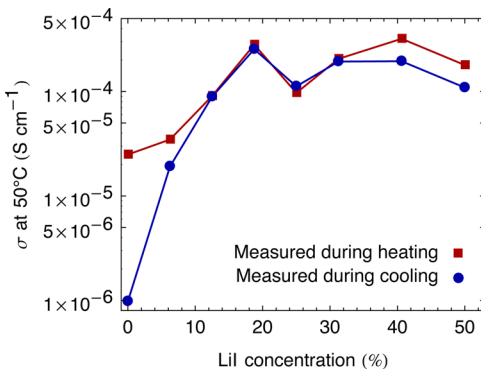


Figure 6. Li^+ conductivity of the $(1-x)\text{LiBH}_4+x\text{LiI}$ samples at 50°C as a function of LiI content for nonannealed (red rectangles) and annealed (blue circles) samples. The data points for pure LiBH_4 (0% LiI content) in this figure are from a measurement on ball-milled LiBH_4 .

solid solution is still at least a factor of 3 away from the 1 mS/cm target.

The conductivity values at 50°C are equal or higher during the heating runs than during the cooling runs. The difference in the conductivity between the heating and the cooling measurements is smallest for samples with LiI content between 18% and 30%. This result is in good harmony with the result shown in Figure 3b, namely, that the particle size and/or density of defects in the nonannealed samples are closest to those in the annealed samples for solid solutions with moderate LiI content.

Together, the XRD and conductivity results indicate that the microstructure of the samples is important for their conductivity and that freshly ball-milled samples with defect-rich microstructure yield higher conductivity values than those in which the defects have been mended by annealing. This is also emphasized by the fact that the measured conductivity does not follow the evolution of the lattice parameter c (see Figure 3a), which has a minimum at a LiI content of 30%. If the left part of Figure 3a is omitted (as it most probably does not reflect the trend of a single phase), one would expect an increase in conductivity in connection with the lattice expansion in the c direction. However, this is not found to be the case here and strongly suggests that a part of the Li^+ conduction might occur along the defects, for example, grain boundaries or dislocations. However, the exact Li^+ conduction mechanism in the $(1-x)\text{LiBH}_4+x\text{LiI}$ solid solution is currently under investigation.

Figure 7 shows the conductivity of the sample with 50% LiI content measured during five consecutive heating and cooling cycles. As shown for the sample with 50% LiI content in Figure 6, the conductivity during cooling is lower than that during heating. However, during the next four temperature cycles, the conductivity performance is very stable and reproducible, confirming the good thermal stability of the HT phase of the solid solution. As explained in Section 2, this sample was prepared and measured using different ball-milling conditions and a different impedance spectroscopy experimental setup than the other samples used in this work. Because the density of defects and particle size are important parameters for the conductivity of the samples, it was to be expected that the conductivity values from this measurement could differ from those presented in Figures 5 and 6. This explains why the conductivity of the sample in Figure 7 is higher at 50°C than

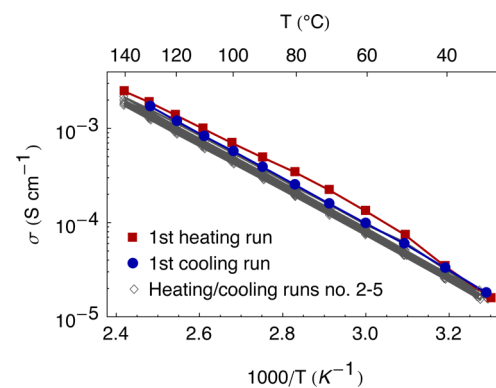


Figure 7. Li^+ conductivity of $\frac{1}{2}\text{LiBH}_4+\frac{1}{2}\text{LiI}$ obtained by impedance spectroscopy during five heating/cooling cycles. The red rectangles and blue circles show the results of the first heating and cooling runs, respectively. The diamonds show the results of the four subsequent heating and cooling cycles.

shown for the sample with 50% LiI content in Figure 6. This also gives an indication of how reproducible the conductivity results are between different laboratory equipment.

4.5. Differential Scanning Calorimetry. Figure 8 shows the results of the DSC measurements. Some of the DSC spectra

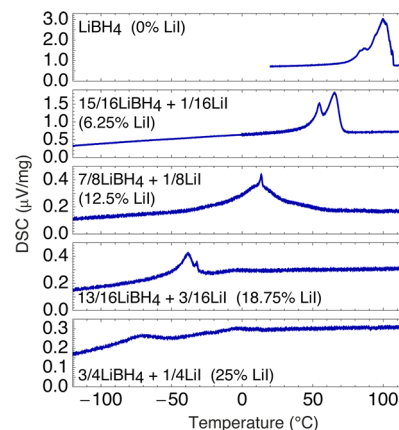


Figure 8. DSC results for different mixing ratios of $(1-x)\text{LiBH}_4+x\text{LiI}$, obtained during cooling.

show two maxima of different intensity, most probably due to microstructural inhomogeneity in the samples. In these cases, the phase transition temperature is taken to be that at which the greater maximum is located.

In Figure 9, the phase transition temperature between the HT and the LT phases of the LiBH_4-LiI system is shown as a function of LiI content. For the measured LiI content, there is a clear linear dependency, with the transition temperature decreasing by approximately 70°C for every 10% of LiI addition. For all measured mixtures with a LiI content equal to or above 12.5%, the transition temperature lies below room temperature.

In Figure 10, the calculated energy differences $\Delta E(x)$ between the HT and LT phases (shown in Figure 1) are plotted against the transition temperatures measured using DSC. Here, x denotes the LiI content of the samples. At each phase transition temperature, the Gibbs free energy difference between the two phases is zero. Since contributions from the zero point energy difference and the volume change between the two phases are small, we set $\Delta H(x) \approx \Delta E(x)$, where

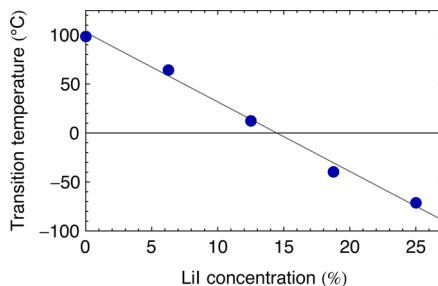


Figure 9. Phase transition temperatures between the hexagonal HT phase and the orthorhombic LT phase in the $(1-x)\text{LiBH}_4+x\text{LiI}$ solid solution as a function of LiI content. For all measured mixtures with $x \geq 12.5\%$, the transition temperature lies below room temperature.

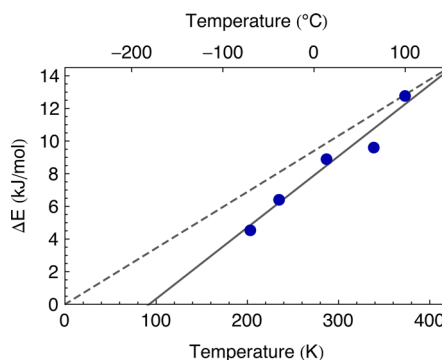


Figure 10. Calculated ground-state energy difference between the HT and the LT structures, $\Delta E(x)$, for different iodine contents x as a function of the measured phase transition temperature. The slopes of the lines in the figure represent the entropy change $\Delta S(x)$ between the two phases. The dashed line shows the limit of $\Delta S(x) = 0$.

$\Delta H(x)$ is the enthalpy change for a given ratio of iodine x . Therefore, we can write

$$\Delta E(x) = T \Delta S(x) \quad (3)$$

As a result, the slopes of the lines in Figure 10 represent the entropy difference ΔS between the two phases.

For the iodine free system, we get an entropy difference between the two phases of $\Delta S(0) = 34.7 \text{ J}/(\text{mol K})$. If the addition of iodine was purely an enthalpy effect, $\Delta S(x)$ should remain constant for the different contents of iodine, and all data points should fall on the dashed line in Figure 10. It is apparent that the entropic difference $\Delta S(x)$ is reduced with addition of iodine by roughly $0.5 \text{ J}/(\text{mol K})$ per percentage point of increased iodine content in the system, but it is not possible to quantify how much should be attributed to the changes in the LT or HT, respectively, resulting from, for example, changes in directional bonding or configurational entropy.

The calculated value of $\Delta E(0) = 12.8 \text{ kJ}/(\text{mol K})$ is also significantly higher than the published enthalpy values from Kharbachi et al.⁵⁰ ($\Delta H_{\text{Kharbachi}} = 5.1 \text{ kJ}/(\text{mol K})$) and Gorbunov et al.⁵¹ ($\Delta H_{\text{Gorbunov}} = 6.2 \text{ kJ}/(\text{mol K})$). This overestimate of the ground-state energy difference also leads to an overestimate of the entropy difference between the two phases. Our calculated value is $\Delta S(0) = 34.4 \text{ J}/(\text{mol K})$ compared to the published values from Pistorius et al.⁵² ($\Delta S_{\text{Pistorius}} = 16.5 \text{ J}/(\text{mol K})$) and from Kharbachi et al.⁵⁰ ($\Delta S_{\text{Kharbachi}} = 13.1 \text{ J}/(\text{mol K})$). Assuming that $\Delta E(x)$ is similarly overestimated, $\Delta S(x)$ should probably be scaled down by a factor of 2.0–2.5. Although $\Delta S(x)$ varies with iodine content, the governing factor comes from the change in the ground-state

energy difference $\Delta E(x)$, which can be used as a predictor for the change in stability between the two phases.

5. SUMMARY AND OUTLOOK

The LiI content and the phase transition temperature between the HT and the LT phases are linearly dependent up to at least 25% LiI content as measured using DSC. A decrease in the transition temperature by $70 \text{ }^{\circ}\text{C}$ for every 10% of LiI addition was found. Density functional theory calculations also show that there is a close to linear stabilization of the HT structure with LiI addition up to a LiI content of 25%. For all samples with a LiI content equal to or greater than 12.5%, the phase transition temperature lies below room temperature, and after ball milling, the samples only contain the HT phase as observed using XRD.

The $(1-x)\text{LiBH}_4+x\text{LiI}$ solid solutions show a high Li^+ conductivity. At $30 \text{ }^{\circ}\text{C}$, the conductivity exceeds 0.1 mS/cm (for the sample with 40% LiI content), and at $140 \text{ }^{\circ}\text{C}$, it exceeds 10 mS/cm (for the sample with 18.75% LiI content) as measured using impedance spectroscopy. Which mixing ratio of $(1-x)\text{LiBH}_4+x\text{LiI}$ yields optimal conductivity depends greatly on which temperature range is in question. The conductivity is equal or higher during heating than during cooling, with the least difference between heating and cooling results for a LiI content between 18% and 30%.

Nonannealed samples with a low LiI content have apparent densities of defects greater than those with a high LiI content, as revealed by analyzing the fwhm of the reflections in the XRD data. This could be an artifact due to the presence of inhomogeneities and/or intermediate phases with similar but different cell parameters. After annealing, the density of defects appears to be almost the same for all samples, but the crystallite sizes grow with increasing LiI content. This could explain why samples with low LiI content tend to have a higher conductivity at high temperature than the samples with low LiI content, emphasizing the importance of the grain boundaries for the conduction mechanism.

The least change between the nonannealed and annealed samples is observed for a LiI content of around 30%. By combining information obtained from XRD and from impedance spectroscopy, it is found that samples with defect-rich microstructure, most probably dislocations and/or grain boundary defects, yield higher conductivity values than those in which the defects have been mended by heat treatment and where only intrinsic point defects might exist. This shows that microstructure and heat treatment are important for the conductivity of the samples. Finally, it is found that the expansion of the lattice parameter c is not a predominant parameter for increased conductivity.

The Li^+ conductivity must be high if the $(1-x)\text{LiBH}_4+x\text{LiI}$ solid solution should be used as an electrolyte in a working battery cell. However, the performance of the electrolyte must also remain stable during the lifetime of the battery. In this work, a LiI content around 30% yields the optimal combined room-temperature performance in terms of microstructural stability under heat treatment and in terms of high Li^+ conductivity. Impedance spectroscopy measurements during five temperature cycles show that the conductivity of the material is stable and reproducible. However, working battery cells using this system as an electrolyte are still to be tested and characterized, and the exact Li^+ conduction mechanism must still be determined.

■ ASSOCIATED CONTENT

§ Supporting Information

Examples of Nyquist plots and additional Arrhenius plots from impedance spectroscopy measurements. This material is available free of charge via the Internet at <http://pubs.acs.org>.

■ AUTHOR INFORMATION

Corresponding Author

*Phone: +45 46775818; fax: +45 4677 5688; e-mail: teve@dtu.dk.

Author Contributions

The manuscript was written through contributions of all authors. All authors have given approval to the final version of the manuscript.

Notes

The authors declare no competing financial interest.

■ ACKNOWLEDGMENTS

The authors would like to acknowledge support from the Copenhagen Graduate School for Nano Science and Technology, COST Action MP1103 “Nanostructured materials for solid-state hydrogen storage”, the Danish Center for Scientific Computing (DCSC), the Center of Atomic-Scale Materials Design (CAMD), and the Energy Research Fund of Landsvirkjun, Iceland.

■ REFERENCES

- (1) Song, J. Y.; Wang, Y. Y.; Wan, C. C. Conductivity Study of Porous Plasticized Polymer Electrolytes Based on Poly(vinylidene fluoride) A Comparison with Polypropylene Separators. *J. Electrochem. Soc.* **2000**, *147*, 3219–3225.
- (2) Nakagawa, H.; Izuchi, S.; Kuwana, K.; Nukuda, T.; Aihara, Y. Liquid and Polymer Gel Electrolytes for Lithium Batteries Composed of Room-Temperature Molten Salt Doped by Lithium Salt. *J. Electrochem. Soc.* **2003**, *150*, A695.
- (3) Knauth, P. Inorganic Solid Li ion Conductors: an Overview. *Solid State Ionics* **2009**, *180*, 911–916.
- (4) Goodenough, J. B.; Kim, Y. Challenges for Rechargeable Li Batteries. *Chem. Mater.* **2010**, *22*, 587–603.
- (5) Tarascon, J.-M.; Armand, M. Issues and Challenges Facing Rechargeable Lithium Batteries. *Nature* **2001**, *414*, 359–67.
- (6) Tarascon, J.-M. Key Challenges in Future Li-Battery Research. *Philos. Trans. R. Soc., A* **2010**, *368*, 3227–41.
- (7) Rabenau, A. Lithium Nitride and Related Materials, Case Study of The Use of Modern Solid State Research Techniques. *Solid State Ionics* **1982**, *6*, 277–293.
- (8) Belous, A. G.; Novitskaya, G. N.; Polyanetskaya, S. V.; Gornikov, Y. I. *Izv. Akad. Nauk SSSR* **1987**, *23*, 470–472.
- (9) Inaguma, Y.; Liquan, C.; Itoh, M.; Nakamura, T.; Uchida, T.; Ikuta, H.; Wakihara, M. High Ionic Conductivity in Lithium Lanthanum Titanate. *Solid State Commun.* **1993**, *86*, 689–693.
- (10) Yang, K.-Y.; Fung, K.-Z.; Leu, I.-C. Study on the Structural Change and Lithium Ion Conductivity for the Perovskite-Type $\text{LaAlO}_3\text{-La}_{0.50}\text{Li}_{0.50}\text{TiO}_3$ Solid Solution. *J. Alloys Compd.* **2007**, *438*, 207–216.
- (11) Bohnke, O. The Fast Lithium-Ion Conducting Oxides $\text{Li}_{3x}\text{La}_{2/3-x}\text{TiO}_3$ From Fundamentals to Application. *Solid State Ionics* **2008**, *179*, 9–15.
- (12) Thangadurai, V.; Schwenzel, J.; Weppner, W. Tailoring Ceramics for Specific Applications: a Case Study of the Development of All-Solid-State Lithium Batteries. *Ionics* **2005**, *11*.
- (13) Aono, H.; Sugimoto, E.; Sadaoka, Y.; Imanaka, N.; Adachi, G. Electrical Property and Sinterability of $\text{LiTi}_2(\text{PO}_4)_3$ Mixed with Lithium Salt (Li_3PO_4 or Li_3BO_3). *Solid State Ionics* **1991**, *47*, 257–264.
- (14) Arbi, K.; Rojo, J. M.; Sanz, J. Lithium Mobility in Titanium Based Nasicon $\text{Li}_{1+x}\text{Ti}_{2-x}\text{Al}_x(\text{PO}_4)_3$ and $\text{LiTi}_{2-x}\text{Zr}_x(\text{PO}_4)_3$ Materials Followed by NMR and Impedance Spectroscopy. *J. Eur. Ceram. Soc.* **2007**, *27*, 4215–4218.
- (15) Bruce, P. G.; West, A. R. The A-C Conductivity of Polycrystalline LISICON, $\text{Li}_{2+2x}\text{Zn}_{1-x}\text{GeO}_4$, and a Model for Intergranular Constriction Resistances. *J. Electrochem. Soc.* **1983**, *130*, 662–669.
- (16) Kamaya, N.; Homma, K.; Yamakawa, Y.; Hirayama, M.; Kanno, R.; Yonemura, M.; Kamiyama, T.; Kato, Y.; Hama, S.; Kawamoto, K.; et al. A Lithium Superionic Conductor. *Nat. Mater.* **2011**, *10*, 682–686.
- (17) Stramare, S.; Thangadurai, V.; Weppner, W. Lithium Lanthanum Titanates: a Review. *Chem. Mater.* **2003**, *15*, 3974–3990.
- (18) Robertson, A. D.; West, A. R.; Ritchie, A. G. Review of Crystalline Lithium-Ion Conductors Suitable for High Temperature Battery Applications. *Solid State Ionics* **1997**, *104*, 1–11.
- (19) Brodd, R. J.; Huang, W.; Akridge, J. R. Polymer Battery R&D in the U.S. *Macromol. Symp.* **2000**, *159*, 229–245.
- (20) Park, M.; Zhang, X.; Chung, M.; Less, G. B.; Sastry, A. M. A Review of Conduction Phenomena in Li-Ion Batteries. *J. Power Sources* **2010**, *195*, 7904–7929.
- (21) Züttel, A.; Rentsch, S.; Fischer, P.; Wenger, P.; Sudan, P.; Mauron, P.; Emmenegger, C. Hydrogen Storage Properties of LiBH_4 . *J. Alloys Compd.* **2003**, *356–357*, 515–520.
- (22) Łodziana, Z.; Vegge, T. Structural Stability of Complex Hydrides: LiBH_4 Revisited. *Phys. Rev. Lett.* **2004**, *93*, 145501.
- (23) Kang, J. K.; Kim, S. Y.; Han, Y. S.; Muller, R. P.; Goddard, W. a. A candidate LiBH_4 for Hydrogen Storage: Crystal Structures and Reaction Mechanisms of Intermediate Phases. *Appl. Phys. Lett.* **2005**, *87*, 111904.
- (24) Łodziana, Z.; Vegge, T. Structural Stability of Complex Hydrides: LiBH_4 Revisited Comment: Łodziana and Vegge Reply. *Phys. Rev. Lett.* **2006**, *97*, 119602.
- (25) Mosegaard, L.; Møller, B.; Jørgensen, J.-E.; Bøsenberg, U.; Dornheim, M.; Hanson, J. C.; Cerenius, Y.; Walker, G.; Jakobsen, H. J.; Besenbacher, F.; et al. Intermediate Phases Observed during Decomposition of LiBH_4 . *J. Alloys Compd.* **2007**, *446–447*, 301–305.
- (26) Blanchard, D.; Shi, Q.; Boothroyd, C. B.; Vegge, T. Reversibility of Al/Ti Modified LiBH_4 . *J. Phys. Chem. C* **2009**, *113*, 14059–14066.
- (27) Lang, J.; Gerhauser, A.; Filinchuk, Y.; Klassen, T.; Huot, J. Differential Scanning Calorimetry (DSC) and Synchrotron X-ray Diffraction Study of Unmilled and Milled LiBH_4 : a Partial Release of Hydrogen at Moderate Temperatures. *Crystals* **2012**, *2*, 1–21.
- (28) Matsuo, M.; Nakamori, Y.; Orimo, S.; Maekawa, H.; Takamura, H. Lithium Superionic Conduction in Lithium Borohydride Accompanied by Structural Transition. *Appl. Phys. Lett.* **2007**, *91*, 224103.
- (29) Epp, V.; Wilkening, M. Fast Li Diffusion in Crystalline LiBH_4 Due to Reduced Dimensionality: Frequency-Dependent NMR Spectroscopy. *Phys. Rev. B* **2010**, *82*, 020301.
- (30) Ikeshoji, T.; Tsuchida, E.; Morishita, T.; Ikeda, K.; Matsuo, M.; Kawazoe, Y.; Orimo, S. Fast-Ionic Conductivity of Li^+ in LiBH_4 . *Phys. Rev. B* **2011**, *83*, 144301.
- (31) Soulié, J.-P.; Renaudin, G.; Černý, R.; K, Y. Lithium Borohydride LiBH_4 I. Crystal Structure. *J. Alloys Compd.* **2002**, *346*, 200–205.
- (32) Miwa, K.; Ohba, N.; Towata, S.; Nakamori, Y.; Orimo, S. First-Principles Study on Lithium Borohydride LiBH_4 . *Phys. Rev. B* **2004**, *69*, 1–8.
- (33) Orgaz, E.; Membrillo, A.; Castañeda, R.; Aburto, A. Electronic Structure of Ternary Hydrides Based on Light Elements. *J. Alloys Compd.* **2005**, *404–406*, 176–180.
- (34) Takahashi, K.; Hattori, K.; Yamazaki, T.; Takada, K.; Matsuo, M.; Orimo, S.; Maekawa, H.; Takamura, H. All-Solid-State Lithium Battery with LiBH_4 Solid Electrolyte. *J. Power Sources* **2013**, *226*, 61–64.
- (35) Maekawa, H.; Matsuo, M.; Takamura, H.; Ando, M.; Noda, Y.; Karahashi, T.; Orimo, S. Halide-Stabilized LiBH_4 , a Room-Temper-

ature Lithium Fast-Ion Conductor. *J. Am. Chem. Soc.* **2009**, *131*, 894–895.

(36) Fischer, D.; Müller, A.; Jansen, M. Existiert Eine Wurtzit-Modifikation Von Lithiumbromid? Untersuchungen Im System LiBr/LiI. *Z. Anorg. Allg. Chem.* **2004**, *630*, 2697–2700.

(37) Oguchi, H.; Matsuo, M.; Hummelshøj, J. S.; Vegge, T.; Nørskov, J. K.; Sato, T.; Miura, Y.; Takamura, H.; Maekawa, H.; Orimo, S. Experimental and Computational Studies on Structural Transitions in the LiBH_4 –LiI Pseudobinary System. *Appl. Phys. Lett.* **2009**, *94*, 141912.

(38) Rude, L. H.; Groppo, E.; Arnbjerg, L. M.; Ravnsbæk, D. B.; Malmkjær, R. a.; Filinchuk, Y.; Baricco, M.; Besenbacher, F.; Jensen, T. R. Iodide Substitution in Lithium Borohydride, LiBH_4 –LiI. *J. Alloys Compd.* **2011**, *509*, 8299–8305.

(39) Miyazaki, R.; Karahashi, T.; Kumatanı, N.; Noda, Y.; Ando, M.; Takamura, H.; Matsuo, M.; Orimo, S.; Maekawa, H. Room Temperature Lithium Fast-Ion Conduction and Phase Relationship of LiI Stabilized LiBH_4 . *Solid State Ionics* **2011**, *192*, 143–147.

(40) Wojdry, M. FITYK: a General-Purpose Peak Fitting Program. *J. Appl. Crystallogr.* **2010**, *43*, 1126–1128.

(41) Patterson, A. L. The Scherrer Formula for X-Ray Particle Size Determination. *Phys. Rev.* **1939**, *56*, 978–982.

(42) Stokes, A. R.; Wilson, A. J. C. The Diffraction of X Rays by Distorted Crystal Aggregates-I. *Proc. Phys. Soc.* **1944**, *56*, 174–181.

(43) Kresse, G.; Furthmüller, J. Efficient Iterative Schemes for ab Initio Total-Energy Calculations Using a Plane-Wave Basis Set. *Phys. Rev. B* **1996**, *54*, 11169.

(44) Perdew, J. J.; Burke, K.; Ernzerhof, M. Generalized Gradient Approximation Made Simple. *Phys. Rev. Lett.* **1996**, *77*, 3865.

(45) Blöchl, P. E. Projector Augmented-Wave Method. *Phys. Rev. B* **1994**, *50*, 17953.

(46) Blöchl, P. E.; Först, C. J.; Schimpl, J. Projector Augmented Wave Method: ab Initio Molecular Dynamics with Full Wave Functions. *Bull. Mater. Sci.* **2003**, *26*, 33.

(47) Bahn, S. R.; Jacobsen, K. W. An Object-Oriented Scripting Interface to a Legacy Electronic Structure Code. *Comp. Sci. Eng.* **2002**, *4*, 56–66.

(48) Beekmans, N. M.; Heyne, L. Correlation between Impedance, Microstructure and Composition of Calcia-Stabilized Zirconia. *Electrochim. Acta* **1976**, *21*, 303–310.

(49) Haile, S. M.; West, D. L.; Campbell, J. The Role of Microstructure and Processing on the Proton Conducting Properties of Gadolinium-Doped Barium Cerate. *J. Mater. Res.* **2011**, *13*, 1576–1595.

(50) El Kharbachi, A.; Nuta, I.; Hodaj, F.; Baricco, M. Above Room Temperature Heat Capacity and Phase Transition of Lithium Tetrahydroborate. *Thermochim. Acta* **2011**, *520*, 75–79.

(51) Gorbunov, V. E.; Gavrichev, K. S.; Zalukaev, V. L.; Sharpataya, G. A.; Baku, M. S. I. Heat Capacity and Phase Transformation of Lithium Borohydride. *Zh. Neorg. Khim.* **1984**, *29*, 2333–2337.

(52) Pistorius, C. W. F. T. Melting and Polymorphism of Lithium Tetrahydroborate to 45 kbar. *Z. Phys. Chem.* **1974**, *88*, 253–263.